# A BOUND DINEUTRON: INDIRECT AND POSSIBLE DIRECT OBSERVATIONS*

Ihor M. Kadenko†, Nadiia V. Sakhno

International Nuclear Safety Center of Ukraine
Department of Nuclear and High Energy Physics, Faculty of Physics
Taras Shevchenko National University of Kyiv
St. Volodymyrs'ka, 64/13, 01601 Kyiv, Ukraine

Barna Biró, András Fenyvesi

HUN-REN Institute for Nuclear Research (ATOMKI)
Bem tér 18/c, 4026 Debrecen, Hungary

Ruslan V. Iermolenko, Olga P. Gogota

Department of Nuclear and High Energy Physics, Faculty of Physics
Taras Shevchenko National University of Kyiv
St. Volodymyrs'ka, 64/13, 01601 Kyiv, Ukraine

*Received 9 November 2023, accepted 5 December 2023, published online 26 February 2024*

This paper deals with summarizing available results to indirectly observe a bound dineutron in the $(n, {}^2n)$ nuclear reactions on $^{159}$Tb and $^{197}$Au and its properties to characterize the dineutron as a unique nucleus with the magic number 2. Upon its full-scope discovery, this could open the row with $N = 2$ in the interactive chart of nuclides. To finalize the existence of a bound dineutron, its decay products must be observed. Therefore, a Geant4 model has been developed to simulate the decay of bound dineutrons and detect electrons as one of the decay products of the dineutron. The results obtained demonstrate that a thoroughly planned experiment could provide a positive assurance for observation of a bound dineutron within the $E_\beta = 190$–$560$ keV energy region of the instrumental beta spectrum.

DOI:10.5506/APhysPolBSupp.17.1-A3

## 1. Introduction

A bound dineutron represents the nucleus, which was known as one of the lightest undiscovered isotopes [1]. For years, the dineutron remained one

* Presented at the Symposium on *New Trends in Nuclear and Medical Physics*, Kraków, Poland, 18–20 October, 2023.

† Corresponding author: IMKadenko@univ.kiev.ua

of the most wanted nuclei to be discovered for much deeper understanding of the strong interaction; for a precise description of the structure of the lightest nuclei and more; and for understanding of the role of the dineutron in Big Bang nucleosynthesis [2], in particular, its role in solving the lithium problem [3]. In 2016 and later in 2020, we published papers devoted to possible and statistically significant observations of a bound dineutron in the $(n,^2n)$ nuclear reaction on $^{159}$Tb [4] and $^{197}$Au [5], accordingly. Both our observations of a bound dineutron were indirect and based on the application of two conservation laws for nuclear reactions: the baryon charge conservation law and the energy conservation law. On the one hand, we observed in the outgoing channel of a nuclear reaction the radioactive nuclei of the isotope, which may be generated only in the $(n, 2n)$ nuclear reaction (the baryon charge observation law). On the other hand, the energies of incident neutrons were somewhat 1.3–2.1 MeV below the threshold of the corresponding $(n, 2n)$ nuclear reactions (the energy conservation law). Should a bound dineutron exist as a neutron-excess bound nucleus, then the most likely decay mode for it would be a beta-minus decay with the formation of the deuteron, electron, and an electron antineutrino [6]. Using an up-to-date theoretical approach, we then made the estimates for the half-life and the end-point energy for the dineutron decay and got the following values: 1,215 s and 560 keV [7]. Having such a very important scientific basis and estimates, one can plan the experiments for direct observation of the dineutron in nuclear reactions on other nuclei-candidates such as $^{181}$Ta, *etc.*

## 2. Theoretical basis for dineutron existence

There were many attempts to discover a bound dineutron upon its very first mention back in the 40s of the last century [8]. Since that time, many different theories have been developed in support of searching for a bound dineutron and, contrary, proving that a bound dineutron could not really exist. Two papers by Migdal and Dyugaev [9, 10] attracted our attention, in which a bound dineutron was theoretically predicted as a state within the potential well but outside of the volume of the heavy nucleus and can behave as a separate light nucleus. Then this phenomenon can be observed in some nuclear reactions and corresponding spectra of several nuclei in the output channels should exhibit the states to be interpreted as dineutrons near the nuclear surface. Moreover, some modern theories do not rule out a bound dineutron system [11].

## 3. Indirect observation of the dineutron and its properties

In support of indirect observations of a bound dineutron, we detected the products of the $^{159}$Tb$(n, {}^2n)^{158g}$Tb nuclear reaction under the follow-

ing conditions: the energy of impinging neutrons was $E_n = 6.85$ MeV; the threshold of the corresponding $^{159}$Tb$(n,2n)$; $^{158g}$Tb nuclear reaction $E_{n-\text{th}} = 8.18$ MeV; and detected gamma rays of $E_\gamma = 944.2$ keV energy due to the decay of $^{158g}$Tb [4]. Similarly, we detected the products of the $^{197}$Au$(n,\ ^2n)^{196g}$Au nuclear reaction for the neutron energy $E_n = 6.22$ MeV; the threshold of the corresponding $^{197}$Au$(n,\ ^2n)^{196g}$Au nuclear reaction $E_{n-\text{th}} = 8.11$ MeV; and detected gamma rays of $E_\gamma = 355.73$ keV energy due to the decay of $^{196g}$Au [5]. In the first experiment, the 944.2 keV gamma peak statistical significance was below 5 sigma. In the second experiment, the 355.73 keV gamma peak was detected with a statistical significance, exceeding 5 sigma. Based on these two observations, one can conclude that we indirectly observed the formation of bound dineutrons in sub-threshold nuclear reactions according to the energy and baryon number conservation laws. Then should the dineutron really exist, we could observe it in the same nuclear reactions on other isotopes.

However, the formation of a bound dineutron would not be similar to the formation of, for instance, the deuteron in the $(n, d)$ nuclear reactions on any nuclei in the input channel. Thus, in Migdal's and Dyugaev's papers [9, 10] certain criteria were derived for nuclei, in the potential fields of which a bound dineutron could be formed.

We calculated these criteria in order to present the lists of very likely, likely, less likely, and unlikely nuclei for the generation of a bound dineutron in the $(n,\ ^2n)$ nuclear reaction and found out that the most likely such nuclei are: $^{150}$Sm; $^{159}$Tb; $^{169}$Tm; $^{197}$Au; $^{181}$Ta, *etc.* [12]. Although these results were obtained much later after our experiments on $^{159}$Tb and $^{197}$Au, they confirmed that our initial selection of nuclei to observe a bound dineutron was intuitively rather correct and lately fully justified.

Having such interesting findings, we attempted to derive the corresponding estimates of the most important properties of a bound dineutron [7] and came up to some of the following of them:

— the dineutron is a bound nucleus in the singlet state;
— the binding energy of the dineutron: $B_{dn} \lesssim 2.5$ MeV ($\cong 2.45$ MeV);
— the decay mode: $^2n \to d + e^- + \tilde{\nu}_e$;
— by definition, the dineutron does not have any excited states and therefore is a pure beta-emitter;
— the end-point energy of the $\beta^-$-spectrum: $E_{\max-dn} \cong 0.56$ MeV;
— the half-lives of the dineutron decay for:
  (a) the G–T transition equals 1,215 s;
  (b) the Fermi transition equals 5,877 s;
— the radius estimate: $r_{dn} \cong 4.1$ fm.

With such estimates, we are now well prepared for the development of corresponding modeling tools to simulate the beta-minus decay mode of a bound dineutron and expect whether we could really observe direct decay of the dineutrons.

## 4. Modeling of direct observation of bound dineutrons

A framework to plan activation method-based experiments in low-energy nuclear physics has been devised by us. It utilizes Geant4 [13–15], TALYS [16], and scripts of Python. The framework calculates partial activities in the sample by employing reaction cross sections computed in TALYS (or accessed from the library), sample parameters, and irradiation traits. The calculated activities are employed to simulate the time flow of initial events. In Geant4, the detectors' event streams are computed based on the initial event stream, from which the anti-coincidences are simulated and spectra generated. The framework utilizes time streams to model the experiment's delay time.

A real sample of high-purity Ta 25×25 mm (99.2825% $^{181}$Ta and 0.7175% $^{93}$Nb) was selected for the study. Simulated measurements were also performed for a sample of the highest-purity $^{181}$Ta (99.99%), a commercially available material. The Ta sample (Fig. 1, yellow highlighting) of 50 $\mu$m thickness was chosen to guarantee its thinness while recording beta particles during the anticipated dineutron decay.

The detector configuration is depicted in Fig. 1 and was selected for the experiment. An estimation of 560 keV is made for the end-point energy of the beta spectrum during dineutron decay. It is crucial that the beta particle energies resulting from dineutron decay are wholly absorbed within the detector volume, but with minimal efficiency for detecting gamma rays in the beta detector. Based on calculations and model adjustment, an organic scintillator with a 5 mm thickness was chosen as the optimal beta detector (Fig. 1, green highlighting). It is necessary to diminish the gamma-ray

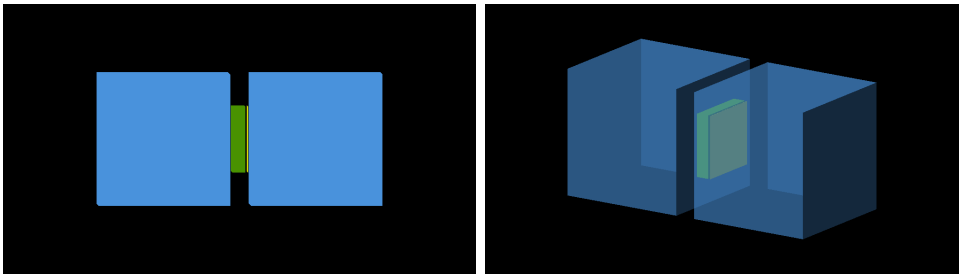

Fig. 1. Detecting system geometry. Sample Ta (yellow) 25 × 25 mm and of 50 $\mu$m thickness, weight — 0.52 g; beta detector (green, organic scintillator) 25×25×5 mm; gamma detectors (blue, anti-coincidence) BGO 50 × 50 mm.

influence when conducting the desired dineutron decay observation. For this reason, an anti-coincidence mode was chosen to suppress the events accompanied by gamma-ray emission. Only events, not accompanied by gamma rays, were recorded in the beta detector.

To enhance the suppression of gamma-ray events, the detection efficiency of gamma detectors should be at its maximum. Therefore, BGO is proposed as the detector material due to its high efficiency for gamma-rays detection. The gamma detectors have dimensions of $50 \times 50 \times 50$ mm, and two detectors are planned to be used, as shown in Fig. 1 (blue highlighting).

Table 1 shows the main irradiation parameters of the Ta sample and the measurement of the induced activity to detect possible dineutron decay. The neutron energy is chosen to be 5.69 MeV because the $^{181}$Ta$(n, 2n)$ reaction channel remains closed. The neutron flux was determined, taking into account the features of the available accelerator-based neutron source [5]. The irradiation time of the sample was chosen to correspond to 4 predicted dineutron half-lives. It is not advisable to increase the irradiation time since the accumulation of $^{182}$Ta nuclei will occur due to the $^{181}$Ta$(n,\gamma)$ reaction, the beta decay of which will complicate the detection of the dineutron. The possible delay time between the end of irradiation and the start of the measurement is 900 s, and this limitation is due to the actual conditions of the experiment at the MGC-20 neutron facility [5].

The measurement time was chosen to be equal to 6 predicted dineutron half-lives.

Table 1. Irradiation and measurement conditions.

| Neutron energy | 5.69 MeV |
|---|---|
| Neutron flux density | $2.7 \times 10^7$ n/cm$^2$ s |
| Irradiation time | 4,860 s ($4 \times T_{1/2}$ of $^2n$) |
| Delay time (between irradiation and measurement) | 900 s |
| Measurement time | 6,075 s ($6 \times T_{1/2}$ of $^2n$) |

Based on the above irradiation and measurement conditions, our framework was used to simulate an experiment for the possible detection of a dineutron. Since there is no dineutron in the databases used by Geant4, it was simulated with $^{90}$Sr since the end-point beta energy of the $^{90}$Sr spectrum is 546 keV, which is quite close to the predicted energy of dineutron decay (560 keV). At the same time, a half-life of 1,215 s was used in modeling the dineutron activity and generation of initial events, which is also a predicted value. In addition, the decay of $^{90}$Sr into $^{90}$Y was blocked.

The TALYS package was used to calculate the cross sections for neutron interaction reactions of a given energy (Table 1) with $^{181}$Ta and $^{93}$Nb. This package does not have a model of the predicted $^{181}$Ta($n$, $^{2}n$)$^{180}$Ta nuclear reaction. Therefore, the channel for this reaction was added separately to the framework with a cross section of 0.1 mb as it was determined in [5] for the nuclear reaction on $^{197}$Au.

The reaction cross sections for $^{181}$Ta and $^{93}$Nb (as a sample impurity) and the accordingly calculated activities at the end of neutron irradiation are presented in Tables 2 and 3.

Table 2. Reaction cross sections for $^{181}$Ta and calculated activities.

| | Reaction product | | | | | | | |
|---|---|---|---|---|---|---|---|---|
| | $^{182}$Ta | $^{182m10}$Ta | $^{178}$Lu | $^{178m3}$Lu | $^{177}$Lu | $^{181}$Hf | $^{2}n$ | $^{180}$Ta |
| Cross section [mb] | 2.071 | 0.209 | 1E-07 | 2.33E-06 | 1E-07 | 3E-03 | 0.1 | 0.1 |
| $T_{1/2}$ [s] | 9,886,752 | 950.4 | 1,704 | 1,386 | 574,301 | 3,662,496 | 1,215 | 29,347.2 |
| Activity [Bq] | 1.8E-02 | 5.689 | 7.48E-05 | 5.96E-05 | 1.64E-08 | 7.73E-05 | 2.628 | 0.304 |

Table 3. Reaction cross sections for $^{93}$Nb and calculated activities.

| | Reaction product | | | | | |
|---|---|---|---|---|---|---|
| | $^{94}$Nb | $^{94m1}$Nb | $^{93m1}$Nb | $^{93}$Zr | $^{90}$Y | $^{90m2}$Y |
| Cross section [mb] | 2.14 | 0.96 | 230.9 | 2.48 | 0.81 | 0.28 |
| $T_{1/2}$ [s] | 6.41E+11 | 3.76E+02 | 5.09E+08 | 4.83E+13 | 2.31E+05 | 1.15E+04 |
| Activity [Bq] | 4.07E-09 | 6.25E-01 | 9.99E-04 | 1.13E-10 | 5.00E-03 | 4.70E-02 |

Preliminary modeling studies indicate a low incidence of events resulting from the beta decay of the dineutron. Since there are technical limitations to increasing the neutron flux and/or sample size, ten irradiations and measurements were simulated each time with another Ta foil, followed by a summation of the spectrum to improve the statistics. The simulated initial events in the sample were modeled using the induced activities and half-lives (Table 2) and the time characteristics of the experiment (Table 1).

For the detector geometry shown in Fig. 1, the interaction of radiation from the sample activities with the detector volumes was modeled in Geant4. The results of the simulation were the flows of events in the detectors. These streams contained a timestamp of the event and the energy absorbed in the detector volume. They were used to generate energy spectra and simulate the anti-coincidence operational mode. The beta particles of the dineutron decay are recorded in the beta detector within the energy range from 190 to 560 keV.

Figure 2 shows the instrumental spectrum of the beta detector corresponding to the registration of all events (blue) and the spectrum of detected events in the beta detector that were not accompanied by events registration in the gamma detectors (orange), *i.e.*, in anti-coincidence mode. In the energy range from 190 to 560 keV, the suppression of events accompanied by gamma ray is $\sim 2.4$ (for $^{181}$Ta sample with Nb impurity).

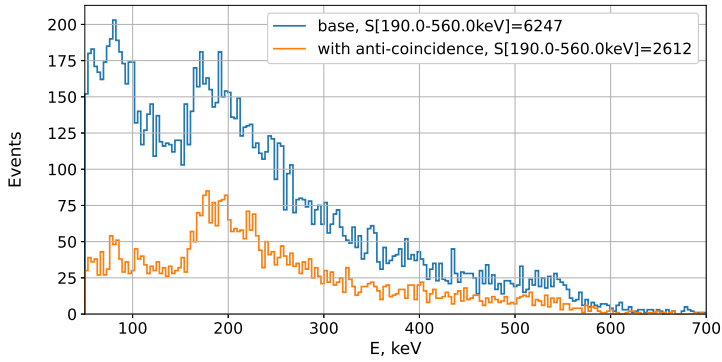


Fig. 2. Anti-coincidences suppression of the original spectrum by a factor of 2.4 (6,247 → 2,612 events) in the energy range of 190–560 keV.

The beta spectrum of the Ta sample after irradiation was then modeled under the condition of dineutron production. The case, when no dineutron is formed, was also modeled. The modeling results are presented in Figs. 3 and 4. The spectra are shown taking into account the operation of the anti-coincidence scheme.

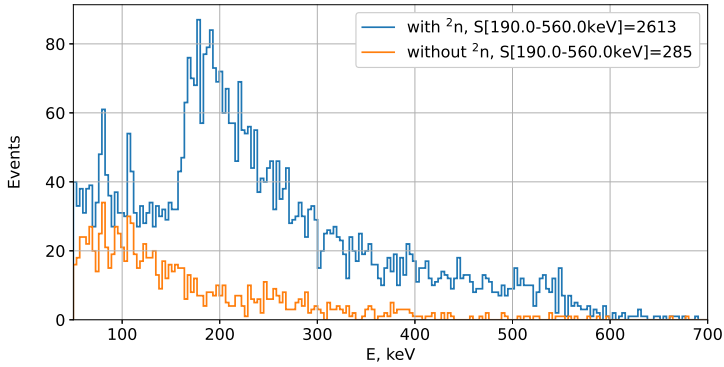


Fig. 3. Detection of $^2n$. The signal-to-background ratio is 9.2 (2,613 → 285 events, sample 99.2825% $^{181}$Ta and 0.7175% $^{93}$Nb) in the energy range of 190–560 keV.

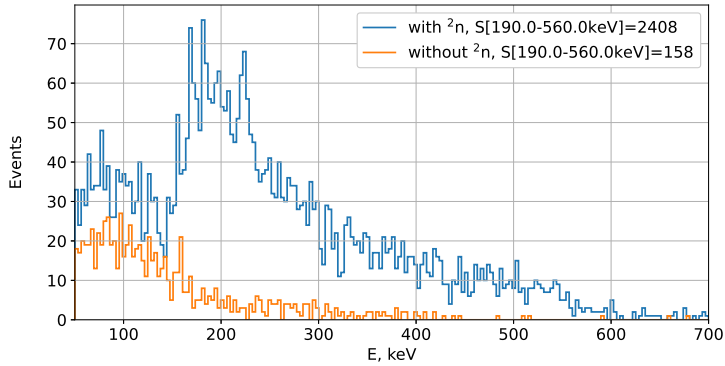


Fig. 4. Detection of $^2n$. The signal-to-background ratio is 15.2 (2,408→158, sample of high-purity 99.99% $^{181}$Ta) in the energy range of 190–560 keV.

## 5. Conclusions

The simulation results demonstrate that it is possible to reliably (signal-to-background ratio is 9.16 for $^{181}$Ta sample with Nb impurity and 15.2 for a sample of high-purity $^{181}$Ta) detect the process of dineutron beta decay, which can be produced by irradiation of $^{181}$Ta with neutrons of 5.69 MeV and a reaction cross section not less than 0.1 mb. Wherein, high purity sample materials are of great importance for such sensitive experiments to ensure successful direct observations of dineutrons even for 30 percent lesser value of the $(n, {}^2n)$ nuclear reaction cross section resulting in lowering signal-to-noise ratio from 15.2 to 9 according to our additional modeling results. Upon the experimental confirmation, such results could shed some light on the discovery of some other multineutron bound systems.

András Fenyvesi received support from the TKP2021-NKTA-42 project financed by the National Research, Development and Innovation Fund of the Ministry for Innovation and Technology, Hungary. The authors thank Boglárka Döncző (ATOMKI, Debrecen, Hungary) for her characterization of the chemical composition of the tantalum sample in the ATOMKI Laboratory for Heritage Science supported by the GINOP-2.3.3-15-2016-00029 'HSLab' project.

## REFERENCES

[1] A.I. Baz, V.I. Gol'danskii, Ya.B. Zel'dovich, *Usp. Fiz. Nauk* **72**, 211 (1960).
[2] D. Nguyen *et al.*, *Phys. Lett. B* **831**, 137165 (2022).
[3] J.P. Kneller, G.C. McLaughlin, *Phys. Rev. D* **70**, 043512 (2004).

[4] I. Kadenko, *Europhys. Lett.* **114**, 42001 (2016).
[5] I.M. Kadenko, B. Biró, A. Fenyvesi, *Europhys. Lett.* **131**, 52001 (2020).
[6] I.M. Kadenko, *Acta Phys. Pol. B* **50**, 55 (2019).
[7] I.M. Kadenko, N.V. Sakhno, O.M. Gorbachenko, A.V. Synytsia, *Nucl. Phys. A* **1030**, 122575 (2023).
[8] M.Y. Colby, R.N. Little, *Phys. Rev.* **70**, 437 (1946).
[9] A.B. Migdal, *Yad. Fiz.* **16**, 428 (1972), [*Sov. J. Nucl. Phys.* **16**, 238 (1973)].
[10] A.M. Dyugaev, *Yad. Fiz.* **17**, 634 (1973).
[11] H.-W. Hammer, S. König, *Phys. Lett. B* **736**, 208 (2014).
[12] N. Dzysiuk, I. Kadenko, O. Prykhodko, *Nucl. Phys. A* **1041**, 122767 (2024).
[13] J. Allison *et al.*, *Nucl. Instrum. Methods Phys. Res. A* **835**, 186 (2016).
[14] J. Allison *et al.*, *IEEE Trans. Nucl. Sci.* **53**, 270 (2006).
[15] S. Agostinelli *et al.*, *Nucl. Instrum. Methods Phys. Res. A* **506**, 250 (2003).
[16] A.J. Koning, D. Rochman, *Nucl. Data Sheets* **113**, 2841 (2012).